Electrical characterization of silicon PV- cell: modeling

Nejmeddine Yahyaoui[1] · Salaheddine Mansouri[2,3] · Abdullah G. Al-Sehemi[4,5,6] · A. Dere[7] · A. Al-Ghamdi[8] ·
Fahrettin Yakuphanoglu[9]

Abstract

The photovoltaic properties of a monocrystalline silicon solar cell were investigated under dark and various illuminations and were modeled by MATLAB programs. According to AM1.5, the studied solar cell has an efficiency rate of 41–58.2% relative to industry standards. The electrical characteristics (capacitance, current–voltage, power-voltage, transient photovoltage, transient photocurrent, and impedance) of a silicon solar cell device were examined. Under complete darkness and light intensity of 100 mW/cm^2, respectively, we have noticed that the light of the AM1.5 spectrum changes all PV-cell parameters such as short current, open circuit voltage, maximum power, maximum voltage, and power conversion efficiency. An electrical equivalent circuit ($R_1//C_1 + R_2//C_2$) was used by the Zview software to fit the experimental data of the Nyquist representations (-Z'' vs. Z'). By analyzing the peak of the conductance G_p versus frequency, the density of interface states and the interface trap time constant were calculated. By using MATLAB programs, we have modeled the current versus voltage and power versus voltage properties of equivalent solar cell circuits, ensuring a good agreement between the experimental and theoretical curves.

1 Introduction

The solar cell is a device that converts the sun's photons into electricity. It's based on different materials that have been drawing a lot of interest over the last decade (Silicon, Silicene, Graphene-TiO$_2$…), due to their potential for more efficient and cost-effective energy production [1–4].

Almost all semiconductor devices sold internationally are made of silicon. Silicon microelectronics devices' excellent performance results from the development of ultramodern technology for electronic systems better-performing, lower-energy large-scale integrated circuits good dependability and consumption. New programs based on in the foreseeable future, silicon is anticipated, further growth of transmission rates, improved information and imagery quality for the applications in the field of communications, restitutions gadgets for games and video, missile technologies, medical systems [5].

✉ Nejmeddine Yahyaoui
  nejmeddine.yahyaoui@ipeis.usf.tn

✉ Salaheddine Mansouri
  mansourislah@gmail.com;
  slaheddinmansori@fstsbz.u-kairouan.tn

1 IPEIS—Institut Préparatoire Aux Etudes d'Ingénieur de Sfax, Université de Sfax, Sfax, Tunisia

2 Faculty of Sciences and Techniques in Sidi Bouzid, Kairouan university, University Campus Agricultural City, 9100 Sidi Bouzid, Tunisie

3 Laboratory of Physics of Materials and Nanomaterials Applied at Environment (LaPhyMNE) LR05ES14, Faculty of Sciences of Gabes, Gabes University, Erriadh City, Zrig, 6072 Gabes, Tunisia

4 Department of Chemistry, Faculty of Science, King Khalid University, P.O. Box 9004, 61413 Abha, Saudi Arabia

5 Research Center for Advanced Materials Science, King Khalid University, P.O. Box 9004, 61413 Abha, Saudi Arabia

6 Unit of Science and Technology, Faculty of Science, King Khalid University, P.O. Box 9004, 61413 Abha, Saudi Arabia

7 Nanoscience and Nanotechnology Laboratory, Firat University, Elazig, Turkey

8 Department of Physics, Faculty of Science, King Abdulaziz University, 21589 Jeddah, Saudi Arabia

9 Physics Department, Faculty of Science, Fırat University, Elazığ, Turkey

The most successful solar cell has been based on crystalline silicon (c-Si), among the numerous competing photovoltaic device technologies, both in terms of shipping and industrial production [6]. 85 percent of photovoltaic devices sold worldwide are solar cells made on crystalline silicon [7]. For the mass manufacture of solar modules for commercial use, crystalline silicon continues to be the material of choice. The crystalline silicon has the inherent advantages of being a plentiful element with a band gap appropriate for photovoltaic conversion and being non-toxic. The fact that it dominates the microelectronics sector has also led to it becoming the semiconductor that has been studied the most, and over the years, various specialized procedures requiring its use have been created and improved. In the photovoltaic ecosystem, silicon monocrystalline solar cells are preferred in terms of market share and performance due to many advantages, including cheap maintenance costs, high reliability, and eco.friendly [8–10].

The most crucial aspect of our lives is represented by optoelectronic gadgets. When light intensity is used to transform electrical current into optical signals, small semiconductor devices are required. For example, light-emitting diodes in radios and other appliances, photodetectors in elevator doors, and laser diodes that carry phone calls through glass fibers [11, 12]. These sophisticated interactions between light and electrons are used by optoelectronic devices. Modern optoelectronic devices frequently contain semiconductor nanometer size structures.

The photoelectric devices only function when there is enough light, unlike the many different kinds of electronic parts. The term "photoelectric device" refers to equipment that produces an electrical signal in reaction to infrared, visible, or ultraviolet light. They are frequently employed in systems that detect objects or encoded data by altering the amount of light that is emitted or reflected. To generate usable electric power, photoelectric sensor can be employed as sun cells. The operation of photoelectric appliances is based on one of the numerous photoelectric effects, in which the liberation of electrons from or inside the absorbing material results from the absorption of light quanta. Inorganic semiconductors have been used to create and commercialize photoelectric devices, as in the decades-old widespread use of photoconductive and photovoltaic sensors in electronics and instrumentation.

Capacitive sensing interfaces have become more often utilized in recent years for human input controllers., appearing in everything from mobile phones to computers and medical devices to industrial controls. Applications for capacitive sensing are prevalent in all fields. The range of things that capacitive sensors may directly sense includes motion, electric field, chemical composition, and many others that can be indirectly turned into motion or dielectric constant, including acceleration, pressure, fluid level, and fluid composition. The detecting circuits convert a change in capacitance into a change in voltage, frequency, or pulse width. The detecting circuits are constructed with conductive sensing electrodes in a dielectric, with excitation voltages of the order of five volts. Additionally, it has been observed that heterojunction devices' light-induced capacitance provides significant information on the interface states and deep states [13].

The silicon solar cell technology can be utilized as a photocapacitive and photoresistive component in modern electrical and optoelectronic appliances. The current and power characteristic, photovoltage, photocurrent, Nyquist diagram, capacitance and conductance were measured and studied with the frequency and power light illumination. The I versus V and P versus V properties of an equivalent solar cell circuit have been simulated. The studied models are then put to use by creating programs in Matlab.

2 Experimental parts

2.1 The preparation of silicon solar cell

To fabricate a silicon solar cell, a p-type silicon polished on one side (250-μm thickness, < 100 > oriented, 1–10 Ω-cm) was used. The surface of the silicon was cleaned by RCA process. Then, etching method was used to clean the silicon wafer. The formation p-n solar cell was performed with a diffusion of the phosphorus into silicon wafer at 850 °C. Boron diffusion was done for back surface field. The antireflection layer was coated junction by plasma enhanced chemical vapor deposition (PECVD) method. The back contact was using evaporation of Al. Ag metal was evaporated using thermal evaporator to prepare top contacts.

The final schematic diagram of the prepared monocrystalline silicon solar cell device is shown in Fig. 1.

2.2 Electrical characterization of the solar cell

All the measurements were performed at room temperature. The electrical characterization of the silicon solar cell was done using a FYTRONIX 9000 semiconductor characterization system including AAA class solar simulator and a FYTRONIX 9000 sourcemeter. The experimental setup technique was established to measure the photocapacitance properties of the solar cell under different illuminations, as shown in Fig. 2. This system is consisted of RLC bridge, home-made holder, tungsten lamp and a closed system. Automatic RLC Bridge (PM 6304 Philips&Fluke) was connected to a special designed holder to measure the cell capacitance C and resistance R under dark and illumination conditions. The studied solar cell is represented on the screen of the bridge by a resistance R connected in parallel
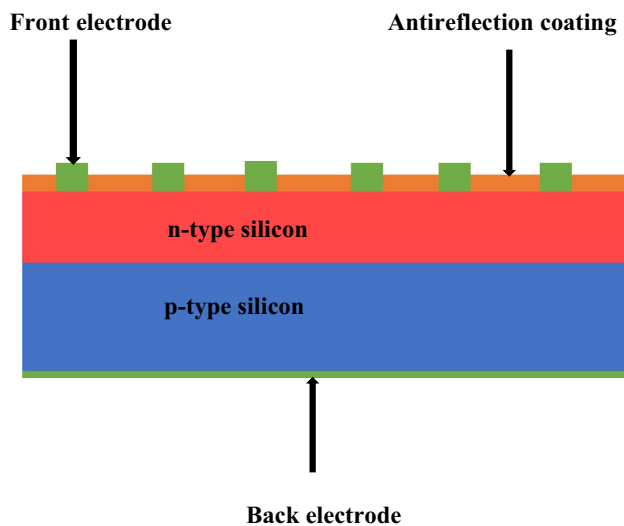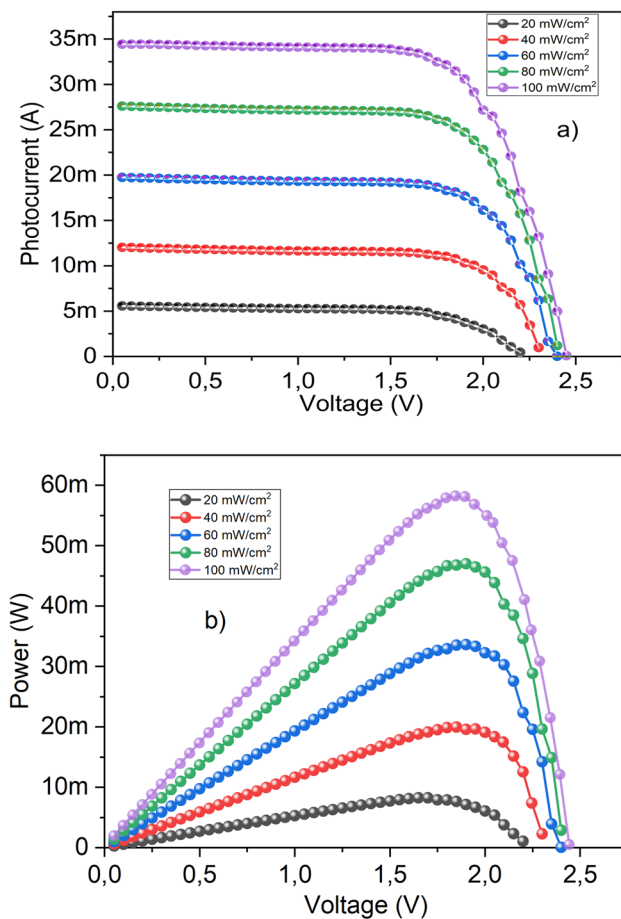
Fig.1 Schematic diagram of silicon solar cell

Fig. 2 **a** I versus V **b** Power versus voltage

with a capacitance C as an equivalent circuit in both dark and illumination conditions. The PM 6304 has a basic accuracy of 0.1%. The maximum resolution for the resistance $R = 0.1$ mΩ and the capacitance C = 0.01 pF. A high power tungsten–halogen lamp which produces a continuous spectrum of light, from near ultraviolet to deep into the infrared region, i.e. 315–2000 nm, was used for photovoltaic and photocapacitance measurements. The distance between the lamp and the sample is approximately equals 30 cm to avoid the heating flow from the lamp to the device.

3 Results and discussion

Photovoltaic parameters of silicon solar cell were measured under white light intensities. In Figs. 2a and b, the characteristics of the I vs V and P vs V curves are shown, respectively. Figure 2a shows a significant difference in the characteristics of I-V. The current is proportional to the flow of intensity light, while the difference in the open circuit voltage increases as the light intensities increase.

Table 1: lists of I_{sc} is the short current, P_{max} is the maximum photovoltaic power, Imax is the maximum photocurrent, fill factor (FF), maximum voltage (V_{max}), PCE is the power conversion efficiency, V_{co} is the open circuit voltage, R_s is the series resistance and R_{sh} is the shunt resistance of silicon solar cells. These variables were all taken from Figs. 2a, b.

A light intensity was used to measure the transient photovoltage and photocurrent curves of silicon solar cells is shown in Fig. 3a, b. The time-dependent generation of charges resulting from the photovoltaic effect was examined using measurements of the transient photovoltage and photocurrent (TPV and TPC) of silicon solar cells. Switching the lighting on and off allowed for the collection of these data. Figure 3a, b displays the TPV and TPC measurements that were made with respect to time and various light intensities. This figure makes it obvious that the photovoltage and photocurrent increased as the intensity of the illumination did. Additionally, Fig. 3 illustrates that the silicon solar cells exhibits the expected switching on/off behavior. The TPV and TPC magnitude climbs quickly up to a specific level and reaches a steady-state value of time after in a relatively short period the lighting condition is "on." This scenario keeps playing out until the light is turned off. When the light source is turned off, the photovoltage and photocurrent magnitude rapidly drops and goes back to its initial value. The carrier's entrapment at the deep levels and the recombination of the extra carriers can be used to explain this

Table 1 Electrical parameter from I-V

	I_{sc} (mA)	V_{oc} (V)	P_{max} (mW)	V_{max} (V)	I_{max} (mA)	FF	PCE %	R_s (Ω)	R_{sh} (Ω)
20 mW/cm²	5	2.20	8.25	1.7	4.85	0.75	41	87.63	2928
40 mW/cm²	12	2.29	19.96	1.85	10.78	0.72	49	32.68	2042
60 mW/cm²	19.74	2.4	33.63	1.9	17.7	0.71	56	19.05	1737
80 mW/cm²	27.6	2.4	47.02	1.9	24.74	0.71	58	15.07	1682
100 mW/cm²	34.4	2.45	58.23	1.85	31.47	0.69	58.2	14.98	917
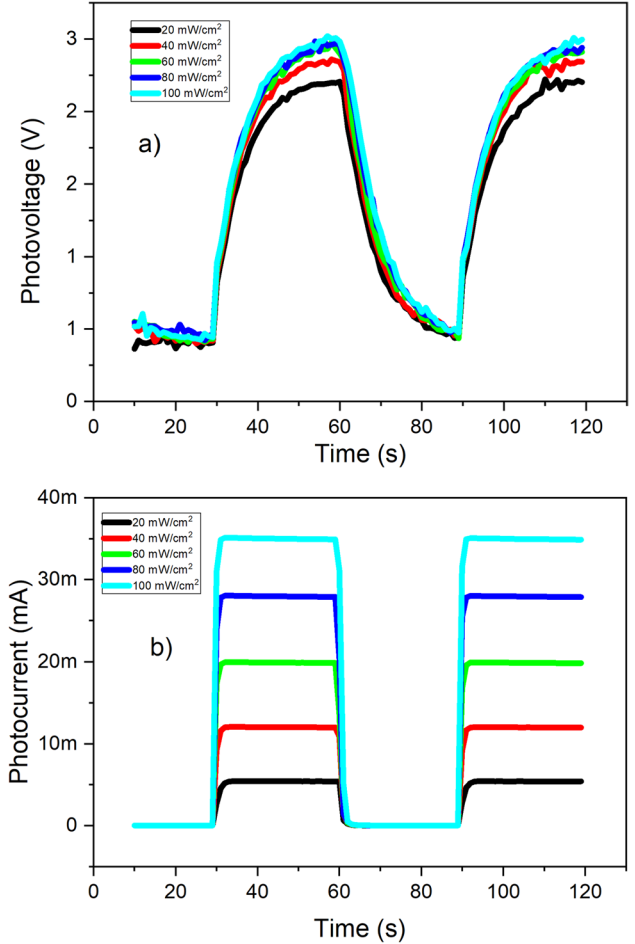
Fig. 3 **a** Transient photovoltage **b** Transient photocurrent
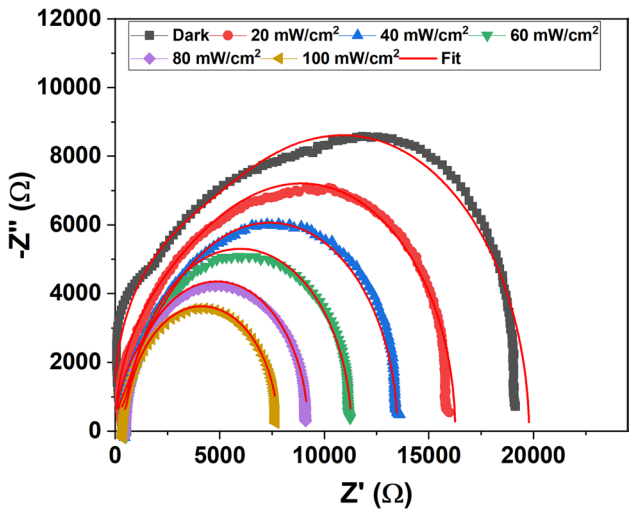
Fig. 4 Nyquist plots fitted using *Zview* software

outcome [14–19]. For the light intensity, the assessment was performed between 20 and 100 mW/cm^2 and the increased photocurrent and photovoltage were obtained for increased illumination. The maximum photocurrent and photovoltage were obtained from light intensity 100 mW/cm^2.

The investigation of solar cells is frequently done using impedance spectroscopy. It is referred to as IS or EIS (electrochemical impedance spectroscopy). It's also known as admittance spectroscopy. By delivering a modest sinusoidal voltage and measuring the current in the frequency domain, it is possible to determine the device's impedance at a number of different frequencies. Due to their distinct transient dynamics, different physical effects in the device can be differentiated by using a wide range of frequencies. For instance, traps may have a stronger effect in the low-frequency band.

In impedance spectroscopy, the solar cell receives a tiny sinusoidal voltage V(t) in accordance with

$$V(t) = V_0 + V_{amp}.sin(\omega t) \tag{1}$$

where $2\pi f$ is the angular frequency, V_0 is the offset voltage, and Vamp is the voltage amplitude. The current density j(t) is also sinusoidal if the voltage amplitude V_{amp} is sufficiently modest, allowing the system to be thought of as linear. For the purpose of distinguishing extrinsic polarization from bulk polarization, impedance analysis was used. A tried-and-true method for identifying and differentiating the dynamics of the many processes that control the electrical response of electronic-optoelectronic system devices is impedance spectroscopy. The measured data were utilized to estimate the parallel and serial combinations of an equivalent circuit model in order to comprehend the complex impedance behavior of the investigated device [20, 21]:

$$Z(\omega) = Z'(\omega) + jZ''(\omega) \tag{2}$$

where Z' represents the real impedance, Z" represents the imaginary impedance, and ω is the angular frequency.

Figure 4: shows Nyquist representations (-Z" vs. Z'). The result of the study displays the presence of semicircular arcs in the entire explored illumination power range. These semicircles are not centered on the real axis, indicating a non-Debye relaxation type [22]. These semicircles diameters decrease as light illumination increases, indicating that the conduction mechanism is thermally activated. By the *Zview* software, these semicircles experimental
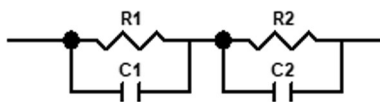
Table 2 Electrical parameters derived from the Nyquist plots fit

Sample	R_1 (Ω)	$C_1 10^{-10}$ (F)	R_2 (Ω)	$C_2 10^{-10}$ (F)	R_T (Ω)
Dark	4520	2.6	14,500	2.3	19,020
20 mW/cm^2	3230	3.8	12,920	3.5	16,150
40 mW/cm^2	1879	5.20	11,617	6.19	13,496
60 mW/cm^2	781	9.20	10,499	9.57	11,280
80 mW/cm^2	564	13.16	8657	18.67	9221
100 mW/cm^2	540	11.78	7238	31.82	7778

data showed good fit using the electrical equivalent circuit ($R_1//C_1 + R_2//C_2$) in Fig. 5. Figure 4 shows good agreement between the experimental and theoretical curves. The electrical parameters are listed in Table 2. It is evident, that when illumination strength increases, the R_1 and R_2 values decrease, which results in the total resistance being reduced. ($R_T = R_1 + R_2$). The total resistance value decreases as the light illumination intensity is raised.
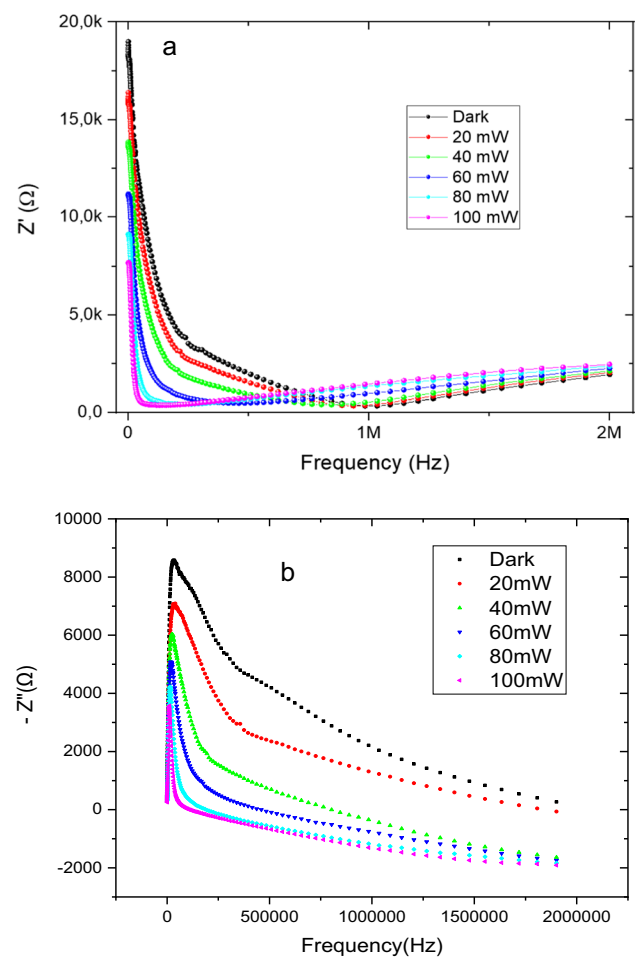

Fig. 5 Equivalent electrical circuit

Fig. 6 a Real impedance versus frequency **b** Complex impedance versus frequency

Given that the intensity of illumination is proportional to the charge generated and, thus, to the charge density, such a decrease does make sense. The relationship between charge density and resistivity is inverse. The resistance should be inversely proportional to the light intensity.

The prepared sample's semiconductor properties are confirmed by a decrease in R_T values.

The real Z' component of the impedance is shown in Fig. 6a as a function of frequency at various light illumination. The amplitude of Z' is higher at the low-frequency, decreases as frequency increases, and is constant at higher frequencies. This might be the result of the behavior of semiconductors, which is an increase in ac-conductivity with frequency. With increasing light illumination, the dispersion zone in the high-frequency region is observed. The real impedance decreases with increasing intensity because the material can be related to space charges by a slow dynamic relaxation process as compared to the dark in the superior frequency field. The value of real impedance shows a decrease with the increase in light intensities.

The imaginary impedance Z'' versus frequency at various light illumination is shown in Fig. 6b. A decrease in peak height should be noted with increasing light intensities. These peaks decrease with increasing light illumination, indicating an increasing loss in the resistive property of the silicon solar cell systems [23].

Using equivalent circuit, we can determine the real and imaginary impedance:

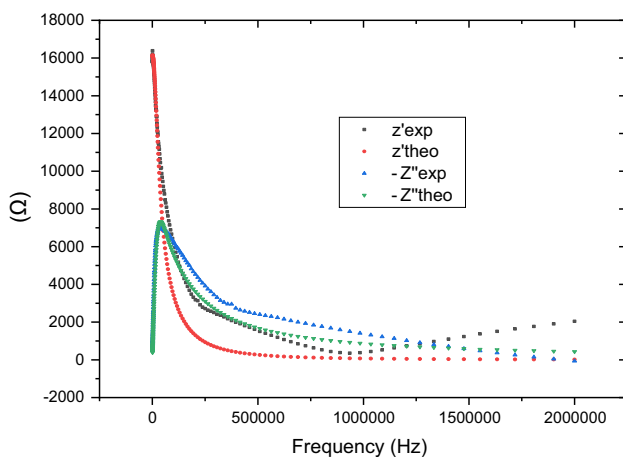$$Z' = \frac{R_1}{1 + \left(R_1 \omega C_1\right)^2} + \frac{R_2}{1 + \left(R_2 \omega C_2\right)^2} \tag{3}$$
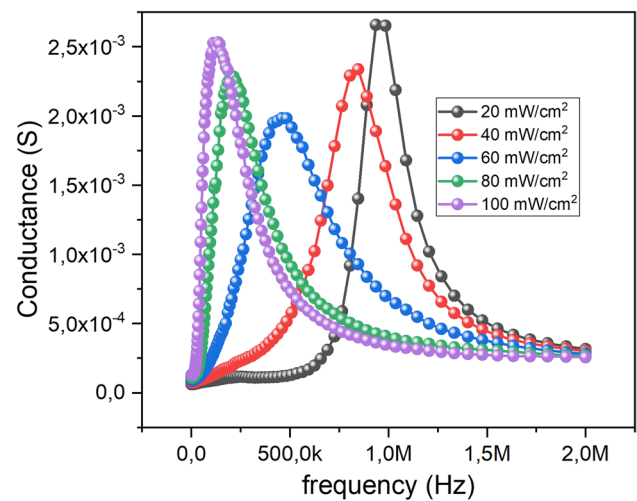

Fig. 8 Conductance versus frequency

and

$$Z'' = -\left(\frac{R_1^2 \omega C_1}{1 + \left(R_1 \omega C_1\right)^2} + \frac{R_2^2 \omega C_2}{1 + \left(R_2 \omega C_2\right)^2}\right) \tag{4}$$

At high frequencies, for each power density, the resistive component approximately approaches zero, and at low frequencies, it is equal to $R_1 + R_2$. At high and low frequencies, the imaginary impedance approaches zero. Excellent agreement between experimental and theoretical curves of real and imaginary impedance is shown in Fig. 7.
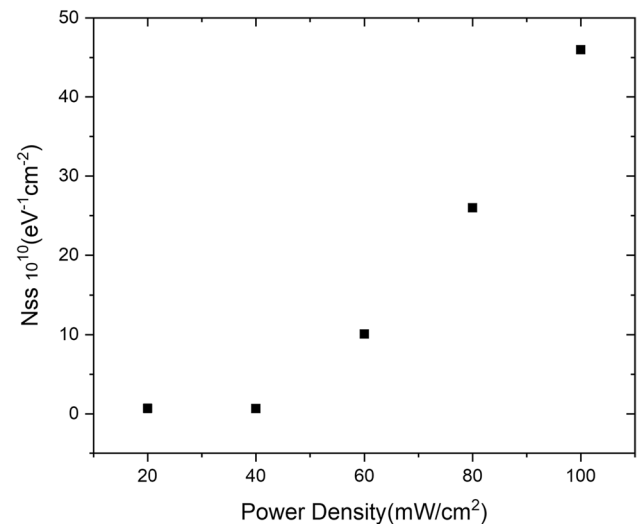

Fig. 7 Experimental and theoretical of imaginary and real impedance versus frequency

Fig. 9 Interface trap density versus light intensities

Fig. 10 Capacitance versus frequency

Fig. 11 Circuit equivalent of silicon diode
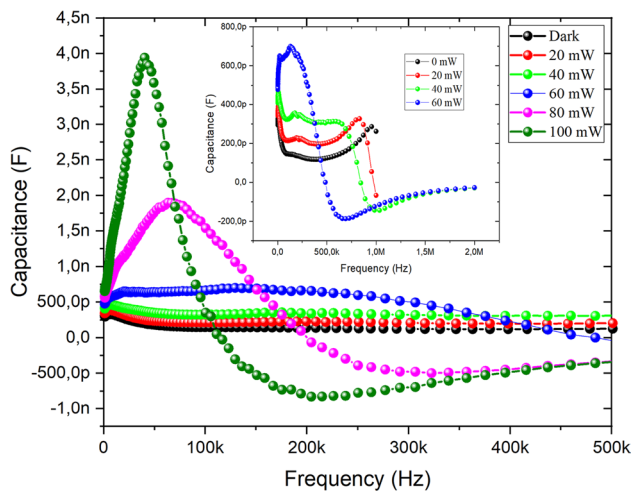
The interface trap states in silicon solar cells have been successfully investigated using frequency dependent conductance measurements. Conductance analysis is mostly useful for resolving the impact of interface trap states on solar cell performance. By examining the silicon solar cells at various frequencies, this method may be used to determine the interface trap density in the depletion and weak inversion section of the band gap as well as the times for the charging and discharging of trap centers. In terms of the maximum conductance, an approximated expression for the interface trap density (N_{ss}) is as follows [24].:

$$N_{ss} = \frac{2.5}{q} \left(\frac{G_p}{\omega} \right)_{max} \qquad (5)$$

where $\omega = 2\pi f$, f, G_p and q are the frequency, conductance and charge of an electron [25]. By analyzing the peak of the G_p versus frequency, the density of interface states and the interface trap time constant can be calculated. Interface traps, which appear at the solar cell interfaces, are exactly responsible for the peak in the G_p versus frequency plot in Fig. 8.

The position of the peak shifts to a low frequency when the power intensities increase. The shift is due to an increase in temperature. Figure 9 shows the interface trap density versus light intensities. The density increases with increasing light intensities.

The capacitance profile versus frequency is shown in Fig. 10. Illumination intensities vary from complete darkness to 100 mW. The capacity varies with frequency as it increases from 0 to 500 kHz, reaching a maximum before declining toward the high values of frequency. Another significant characteristic of this cell is that it has white illumination intensities that transition from positive to negative capacity after 20 mW. In the wide range of the white
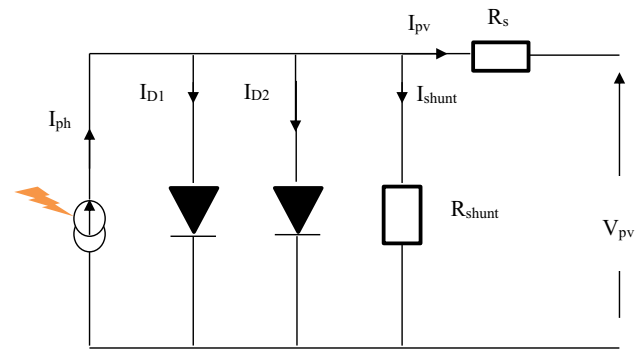
illumination intensities, clearly seen with an illumination intensity of 100 mW, the capacitance decreases rapidly from 4 pF to -1 pF. As illumination intensities and frequencies increase, the capacitance increases and decreases respectively because of the photogenerated charge carriers. At lower frequencies, the drastic increase in capacitance is probably due to the space charge polarization by the increasing number of the photogenerated carriers. The photocapacitance signal is related to both the electric field and the transport properties of photogenerated charges. The variation of capacitance with frequency is strong at lower frequencies, which indicates the presence of interface states at the junction. The capacitance remains almost constant up to a certain value of the frequency at higher frequencies. At lower frequencies, the values of capacitance are attributed to the excess capacitance resulting from the interface states in equilibrium with p-Si that can follow the ac-signal [26]. At the intermediate frequency, the capacitance decrease means that the small part of the interface states can only follow the ac-signal [27, 28]. The values of the capacitance depend on some parameters such as the density of interface states, the thickness, and the series resistance. The increase in the charge carrier concentration under illumination leads to an improvement of the space charge layer [29]. A considerable increase in junction capacitance is taken place because of the number of radiation induced deep defects in this device [30]. Due to thermal annealing [31] and/or illumination with light, these defects heal out restoring to a large extend the initial device performance.

4 Modeling

A silicon-based PV solar cell with a double diode is shown as an equivalent circuit in Fig. 11. This solar cell is modulated, as seen in the figure, by a photocurrent: I_{ph} source that is sensitive to light illumination, a diodes (D) with the ideality factor (n1 and n2) to modulate the loss in junction,
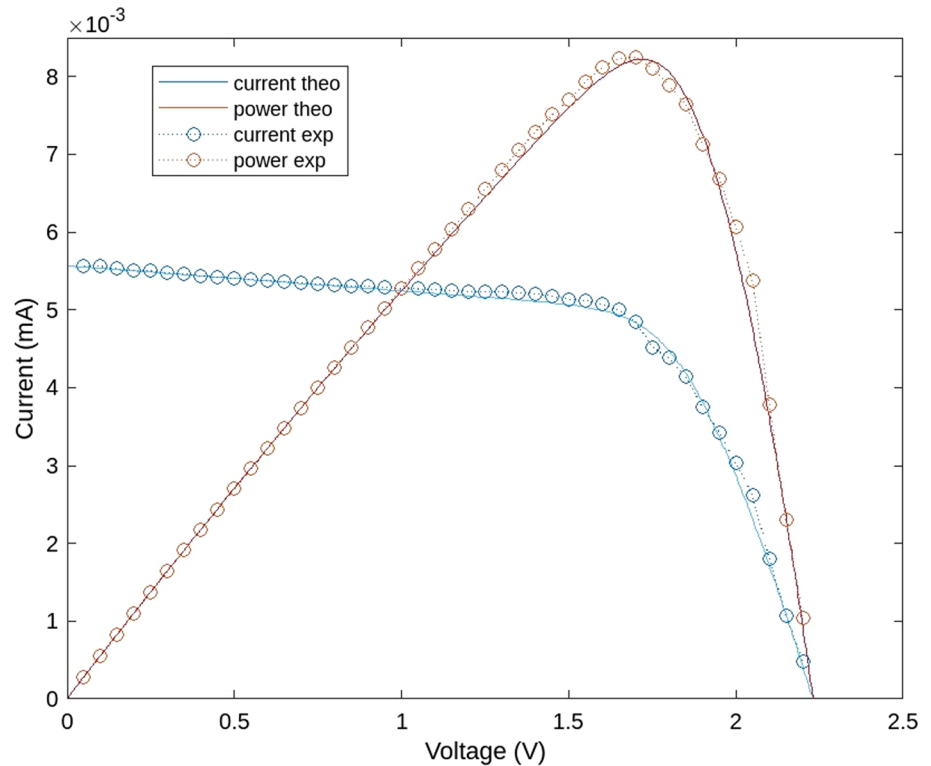
and a shunt resistance: R_{shunt} positioned in parallel with the diode to correspond to the frame of internal resistive losses. A shunt current I_{sh} crosses this shunt resistance. Additional losses caused by the joule effect are simulated by a sequence of resistances Rs [32]. In investigations on PV cells, the seven electrical parameter circuit is widely utilized [23–37]. The double-diode model (I_{ph}, R_{shunt}, n_1, n_2, Is_1, Is_2 and Rs) is predicated on the idea that there are no losses caused by carriers charge recombination in the zone of depletion and that the voltage V at the terminals is all that controls the current produced by photovoltaic cells. The following relation is used to determine the sum of currents following nodal rule manipulation:

$$I_{ph} - I_{D1} - I_{D2} - I_{shunt} - I_{pv} = 0 \tag{7}$$

The voltage across the junction is given by the formula:

$$V_D = V_{pv} + R_s \times I_{pv} \tag{8}$$

where, $I_{shunt} = \frac{V_{pv}+R_s I_{pv}}{R_{shunt}}$, $I_{D1} = I_{s1}\left[e^{\frac{q\left(V_{pv}+R_s I_{pv}\right)}{n1kT}} - 1\right]$ and

$$I_{D2} = I_{s2}\left[e^{\frac{q\left(V_{pv}+R_s I_{pv}\right)}{n2kT}} - 1\right] \tag{9}$$

The following Ipv expression as a function of Vpv results from combining the aforementioned equation.:

$$I_{pv} = I_{ph} - I_{s1}\left[e^{\frac{q\left(V_{pv}+R_s I_{pv}\right)}{n1KT}} - 1\right] - I_{s2}\left[e^{\frac{q\left(V_{pv}+R_s I_{pv}\right)}{n2KT}} - 1\right] - \frac{V_{pv}+R_s I_{pv}}{R_{shunt}} \tag{10}$$

In this equation, $I_{ph:}$ is the photoelectric current, Is is the saturation current, k_b is the Boltzmann constant, T is the junction temperature, n_1 and n_2 are ideality parameters of the diodes, q is the electron charge, R_s and S_{hunts} are the corresponding series and shunt resistances. An efficient agreement between the experimental and theoretical curves is shows in Fig. 12.

5 Conclusion

In this paper, the current voltage (I-V), imaginary part-real part (-Z'' vs. Z'), and conductance-frequency (G-F) measurements were realized to analyze the electrical properties of a silicon solar cell. The current–voltage (I-V) performance of the studied silicon solar cell was measured, and its efficiency was found to be 58.2% at 100 mW/cm2. An electrical equivalent circuit (R1//C1 + R2//C2) was used by the Zview software to fit the experimental data of the Nyquist representations (-Z'' vs. Z'), resulting in good agreement between the experimental and theoretical curves. By analyzing the peak of the conductance G_p versus frequency, the

density of interface states and the interface trap time constant were calculated. The value of the interface trap density increases with increasing light intensities. The capacitance profile increases with increasing illumination intensities and decreases with the increasing frequencies due to the photogenerated charge carriers under the illumination. The drastic increase in capacitance at lower frequencies is probably due to the space charge polarization by the increasing number of the photogenerated carriers. The photocapacitance signal is related to both the electric field and the transport properties of photogenerated charges. By using the double-diode model, $(I_{ph}, I_{s1}, R_{shunt}, n_1, n_2, I_{s2}, $ and $R_s)$ by Matlab programs, we have a good accordance between the experimental and theoretical curves (I-V).

Availability of data and material Not applicable.

Code availability Not applicable.

Declarations

Conflict of interest statement The authors declare that there is no conflict of interest regarding the publication of this article.

Ethical approval The authors declare that they have no known competing financial interests or personal relationships that could have appeared to influence the work reported in this paper.

References

1. Chander S, Purohit A, Sharma A, Arvind, Nehra SP, Dhaka MS (2015) A study on photovoltaic parameters of mono-crystalline silicon solar cell with cell temperature, Energy Rep. 1: 104-109. https://doi.org/10.1016/j.egyr.2015.03.004

2. G. Mnasri, S. Mansouri, M. Yalçinc, L. El Mir, A.A. Al-Ghamdi, F. Yakuphanoglu, Characterization and study of CdS quantum dots solar cells based on Graphene-TiO$_2$ nanocomposite photoanode. Results Phys. **18**, 103253 (2020). https://doi.org/10.1016/j.rinp.2020.103253

3. P. Aghdasi, S. Yousef, R. Ansari, M. Bagheri Tagani, A DFT investigation on the mechanical and structural properties of silicene nanosheets under doping of transition metals. Appl. Phys. A **128**, 716 (2022). https://doi.org/10.1007/s00339-022-05859-5

4. P. Aghdasi, S. Yousefi, R. Ansari, A DFT investigation on the mechanical and structural properties of halogen-and metal-adsorbed silicene nanosheets. Mater. Chem. Phys. **283**, 126029 (2022). https://doi.org/10.1016/j.matchemphys.2022.126029

5. P. Mialhe, H. Toufik, M. Tahchi, N. Toufik, W. Tazibt, Silicon for optoelectronic. J Electron Devices **6**, 170 (2008)

6. J.K. Rath, Low temperature polycrystalline silicon: a review on deposition. Sol. Energy Mater. Sol. Cells **76**, 431 (2003). https://doi.org/10.1016/S0927-0248(02)00258-1

7. J.F. Nijs, J. Szlufcik, J. Poortmans, S. Sivoththaman, R.P. Mertens, Advanced cost-effective crystalline silicon solar cell technologies. Sol. Energy Mater. Sol. Cells **65**, 249 (2001). https://doi.org/10.1016/S0927-0248(00)00100-8

8. E. Cuce, P.M. Cuce, T. Bali, An experimental analysis of illumination intensity and temperature dependency of photovoltaic cell parameters. Appl. Energy **111**, 374–382 (2013). https://doi.org/10.1016/j.apenergy.2013.05.025

9. S.K. Sharma, H. Im, D.Y. Kim, R.M. Mehra, Review on Se-and S-doped hydrogenated amorphous silicon films, Indian J. Pure. Appl. Phys. **52**, 293–313 (2014)

10. P. Singh, N.M. Ravindra, Temperature dependence of solar cell performance-an analysis. Sol. Energy Mater. Sol. Cells **101**, 36–45 (2012). https://doi.org/10.1016/j.solmat.2012.02.019

11. M.A. Green, K. Emery, Y. Hishikawa, W. Warta, Solar cell efficiency tables (version 33). Prog. Photovoltaics Res. Appl. **17**, 85–94 (2009). https://doi.org/10.1002/pip.880

12. S. Günes, H. Neugebauer, N.S. Sariciftci, Conjugated polymer based organic solar cells. Chem. Rev. **107**, 1324–1338 (2007). https://doi.org/10.1021/cr050149z

13. G.B. Sakr, I.S. Yahia, Effect of illumination and frequency on the capacitance spectroscopy and the relaxation process of p-ZnTe/n-CdMnTe/GaAs magnetic diode for photocapacitance applications. J. Alloys Compd. **503**, 213 (2010). https://doi.org/10.1016/j.jallcom.2010.04.235

14. C.A. Arredondo, G. Gordillo, Photoconductive and electrical transport properties of AgInSe$_2$ thin films prepared by co-evaporation. Phys. B **405**, 3694 (2010). https://doi.org/10.1016/j.physb.2010.05.068

15. A. Dere, B. Coskun, A. Tataroglu, A.G. Al-Sehemi, A.A. Al-Ghamdi, Hind M.A. Alateeq, R. Qindeel, W.A. Farooq, F. Yakuphanoglu, Boron doped graphene based linear dynamic range photodiode, Phys. B 545 (2018) 86. https://doi.org/10.1016/j.physb.2018.05.046

16. J.C. Moore, C.V. Thompson, A phenomenological model for the photocurrent transient relaxation observed in ZnO-based photodetector devices. Sensors **13**, 9921 (2013)

17. C.R. McNeill, I. Hwang, N.C. Greenham, Photocurrent transients in all-polymer solar cells: Trapping and detrapping effects. J. Appl. Phys. **106**, 024507 (2009)

18. J. Bao, I. Shalish, Z. Su, R. Gurwitz, F. Capasso, X. Wang, Z. Ren, Photoinduced oxygen release and persistent photoconductivity in ZnO nanowires. Nanoscale Res. Lett. **6**, 404 (2011)

19. F. Teng, K. Hu, W. Ouyang, X. Fang, Photoelectric detectors based on inorganic p-type semiconductor materials. Adv. Mater. **30**, 1706262 (2018)

20. X.F. Wei, W.M. Grill, Impedance characteristics of deep brain stimulati on electrodes in vitro and in vivo. J. Neural Eng. **6**, 046008 (2009). https://doi.org/10.1088/1741-2560/6/4/046008

21. R. Anil Kumar, M.S. Suresh, J. Nagaraju, Facility to measure solar cell ac parameters using an impedance spectroscopy technique. Rev. Sci. Instrum. **72**, 3422–3426 (2001). https://doi.org/10.1063/1.1386632

22. A. Shukla, R.N.P. Choudhary, A.K. Thakur, J. Phys. Chem. Solid **70**, 1401 (2009)

23. A. Bouzidi, W. Jilani, I.S. Yahia, Impedance spectroscopy of monocrystalline silicon solar cells for photosensor applications: highly sensitive device. Physica B **596**, 412375 (2020)

24. M. Cakar, N. Yldrm, H. Dogan, A. Turut, The conductance and capacitance– frequency characteristics of Au/pyronine-B/p-type Si/Al contacts. Appl. Surf. Sci. **253**, 3464–3468 (2007)

25. I. Hussain, M.Y. Soomro, N. Bano, O. Nur, M. Willander, Interface trap characterization and electrical properties of Au-ZnO nanorod Schottky diodes by conductance and capacitance methods. J. Appl. Phys. **112**, 064506 (2012). https://doi.org/10.1063/1.4752402

26. M. Zamora, G.K. Reeves, G. Gazeckia, J. Mi, C.Y. Yang, Measurement of interface states parameters of $Si_{1-x-y} Ge_x C_y$/TiW Schottky contacts using Schottky capacitance spectroscopy. Solid-State Electron. **43**, 801–808 (1999)

27. S. Aydogan, K. Cinar, H. Asıl, C. Cos-kun, A. Türüt, Electrical characterization of Au/n-ZnO Schottky contacts on n-Si. J. Alloys Compd. **476**, 913–918 (2009)

28. A. Ashery, A.A.M. Farag, R. Mahani, Structural, electrical and magnetic characterizations of Ni/Cu/p-Si Schottky diodes prepared by liquid phase epitaxy. Microelectron. Eng. **87**, 2218–2224 (2010)

29. M. Burgelman, P. Nollet, Admittance spectroscopy of thin film solar cells. Solid State Ionics **176**, 2171–2175 (2005)

30. A. Jasenek, U. Rau, Defect generation in Cu(In, Ga)S$_e$2 heterojunction solar cells by high-energy electron and proton irradiation. J. Appl. Phys. **90**, 650–658 (2001)

31. M. Garin, U. Rau, W. Brendle, I. Martin, R. Alcubilla, Characterization of a-Si:H/c-Si interfaces by effective-lifetime measurements. J. Appl. Phys. **98**, 093711–093719 (2005)

32. J. Prasanth Ram, T. Sudhakar Babu, N. Rajasekar, Renew. Sustain. Energy Rev. **67**, 826 (2017). https://doi.org/10.1016/j.rser.2016.09.076

33. A. Orioli, A. Di Gangi, A procedure to evaluate the seven parameters of the two-diode model for photovoltaic modules. Renewable Energy **139**, 582–599 (2019). https://doi.org/10.1016/j.renene.2019.02.122

34. Abdelhady Ramadan. Salah Kamel. Ibrahim B. M. Taha and Marcos Tostado‑Véliz. Parameter Estimation of Modified Double-Diode and Triple-Diode Photovoltaic Models Based on Wild Horse Optimizer, Electronics 10 (2021) 2308. https://doi.org/10.3390/electronics10182308

35. Tanvir Ahmad, Sharmin Sobhan, Md. Faysal Nayan. Comparative Analysis between Single Diode and Double Diode Model of PV Cell: Concentrate Different Parameters Effect on Its Efficiency, Journal of Power and Energy Engineering4 (2016) 31–46. DOI: https://doi.org/10.4236/jpee.2016.43004

36. G. Sulyok, J. Summhammer, Extraction of a photovoltaic cell's double-diode model parameters from data sheet values. Energy Sci Eng. **6**, 1–11 (2018). https://doi.org/10.1002/ese3.216

37. O.S. Elazab, H.M. Hasanien, M.A. Elgendy, A.M. Abdeen, Parameters estimation of single- and multiple-diode photovoltaic model using whale optimisation algorithm. The Institution of Engineering and Technology **12**, 1755–1761 (2018)

CORRECTION

Correction: Electrical characterization of silicon PV-cell: modeling

Nejmeddine Yahyaoui[1] · Salaheddine Mansouri[2,3] · Abdullah G. Al-Sehemi[4,5,6] · A. Dere[7] · A. Al-Ghamdi[8] · Fahrettin Yakuphanoglu[9]

Correction: Applied Physics A 130:379 (2024)
https://doi.org/10.1007/s00339-024-07523-6

In Figs. 6a and 7 of this article, incorrect minus sign were included in "z′". Correct Figs. 6, 7 should have appeared as shown below.

The original article has been corrected.

✉ Nejmeddine Yahyaoui
nejmeddine.yahyaoui@ipeis.usf.tn

✉ Salaheddine Mansouri
mansourislah@gmail.com;
slaheddinmansori@fstsbz.u-kairouan.tn

1 IPEIS—Institut Préparatoire Aux Etudes d'Ingénieur de Sfax, Université de Sfax, Sfax, Tunisia

2 Faculty of Sciences and Techniques in Sidi Bouzid, Kairouan University, University Campus Agricultural City, 9100 Sidi Bouzid, Tunisie

3 Laboratory of Physics of Materials and Nanomaterials Applied at Environment (LaPhyMNE) LR05ES14, Faculty of Sciences of Gabes, Gabes University, Erriadh City, Zrig, 6072 Gabes, Tunisia

4 Department of Chemistry, Faculty of Science, King Khalid University, P.O. Box 9004, 61413 Abha, Saudi Arabia

5 Research Center for Advanced Materials Science, King Khalid University, P.O. Box 9004, 61413 Abha, Saudi Arabia

6 Unit of Science and Technology, Faculty of Science, King Khalid University, P.O. Box 9004, 61413 Abha, Saudi Arabia

7 Nanoscience and Nanotechnology Laboratory, Firat University, Elazig, Turkey

8 Department of Physics, Faculty of Science, King Abdulaziz University, 21589 Jeddah, Saudi Arabia

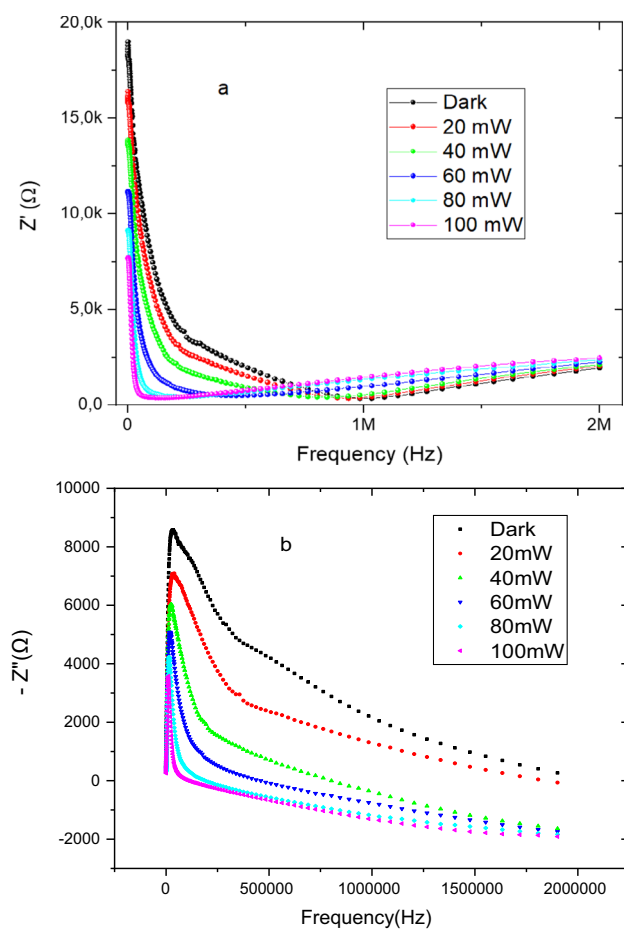9 Physics Department, Faculty of Science, Fırat University, Elazığ, Turkey

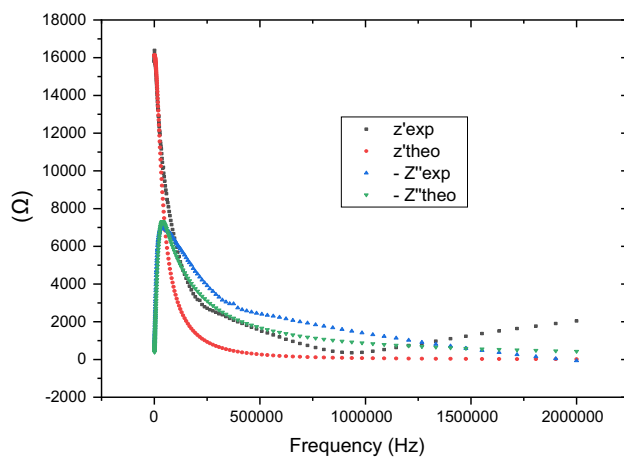**Fig. 6 a** Real impedance versus frequency. **b** Complex impedance versus frequency

Fig. 7 Experimental and theoretical of imaginary and real impedance versus frequency